Applied Surface Science 258 (2011) 76–80

Contents lists available at ScienceDirect

Applied Surface Science

journal homepage: www.elsevier.com/locate/apsusc

The effect of pre-pattern on the morphology and growth speed of TiO_2 nanotube

Tao Xu, Jia Lin, Jingfei Chen, Xianfeng Chen*

Department of Physics; The State Key Laboratory on Fiber Optic Local Area Communication Networks and Advanced Optical Communication Systems, Shanghai Jiao Tong University, 800 Dongchuan Rd. Shanghai 200240, China

ARTICLE INFO

Article history:
Received 27 May 2011
Received in revised form 2 August 2011
Accepted 2 August 2011
Available online 6 August 2011

Keywords:
Nanotube
TiO_2
Pre-pattern
Mechanical etching
Morphology

ABSTRACT

In this work, we presented a new method which directly acts on the surface of the Ti sheet by mechanical micro-etching using a grating ruling engine. The effect of the pre-pattern on the morphology and growth speed of TiO_2 nanostructure formed on the Ti sheet with the traditional anodization method was investigated. A novel wall structure was observed and the growth speed of TiO_2 nanotube (NT) was greatly affected by the pre-pattern. The wall structure increases the surface-to-volume ratio of the nanotube arrays. The new method provided the possibility of further optimization of fast growth of TiO_2 nanostructure and improving the efficiency of dye-sensitized solar cell (DSSC) and photocatalysis.

1. Introduction

TiO_2 nanostructure has drawn increased attentions as it shows great prospects in photocatalysis [1–4], water photoelectrolysis [5–7], gas sensors [8–10], dye-sensitized solar cell (DSSC) [11–14], bio-materials [15,16], etc. Since the pioneering findings of the TiO_2 nanostructure used in the DSSC by Gräzel in 1991 [11], which indicated a new revolutionary method to utilize the solar energy, DSSC has attracted wide attentions, in which the TiO_2 nanoparticle acted as an important carrier of dyes and the transmitter of electrons. In order to improve the efficiency of the TiO_2 nanostructure based DSSC, many studies have been done and a series of fabrication techniques have been proposed, such as sol–gel fabrication [17,18], anodic oxidization [19], hydrothermal synthesis [20], template synthesis [21] and photoelectrochemical etching [22]. Different kinds of morphologies for the TiO_2 nanosrtucture were achieved with above fabrication approaches, such as TiO_2 nanoparticles [23], nanodots/nanorods [24], nanotube (NT) arrays [25], etc. Although researches demonstrate that TiO_2 nanotubes (NTs) based DSSC will have greater potential in enhancing the efficiency [13], large scale and well-ordered TiO_2 NTs with long tube length are rarely fabricated due to the difficulty in controlling the micro-morphology of the TiO_2 NTs during the growth process. As former studies provided comparative mature methods in fabrication of highly ordered nanostructure in anodic alumina oxide (AAO) [26], it is a natural idea to transfer these methods to the fabrication of well-ordered TiO_2 nanostructure [24,27]. There are also some methods to fabricate TiO_2 NTs using the highly ordered AAO or ZnO membranes as templates [21,28]. These methods can be summarized as pre-pattern of the titanium's surface and guided growth of TiO_2 nanostructure. However, because of the different metal and crystalline features between alumina and titanium, and the titanium has greater stability and is more resistant to corrosion, the results are not so satisfactory.

In this paper, we use a new method which directly acts on the surface of titanium as pre-pattern by mechanical micro-etching with a grating ruling engine and then anodize the pre-patterned titanium using the traditional anodization method based on the fluorine contained ethylene glycol electrolyte. We found that the growth speeds and the morphologies of TiO_2 NTs of these samples had great differences, and a series of walls which were made up by TiO_2 NTs were formed on the mechanically micro-etched samples.

2. Experimental

To study the influence of pre-pattern on the formation of TiO_2 NT, Ti sheet (99.6% purity, 0.2 mm thickness, Strem Chemicals) was used and four kinds of Ti sheets (2 cm × 5 cm) with different methods were prepared, named sample a, b, c and d. Sample a was mechanically polished and then mechanically etched by a grating ruling engine to form a series of grooves with an interval of 1 μm

* Corresponding author. Tel.: +86 21 54743252; fax: +86 21 54743273.
E-mail address: xfchen@sjtu.edu.cn (X. Chen).

0169-4332/$ – see front matter © 2011 Elsevier B.V. All rights reserved.
doi:10.1016/j.apsusc.2011.08.008

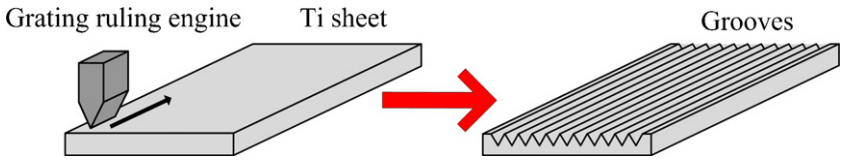

Fig. 1. Schematic illustration of mechanical micro-etching of the Ti sheet's surface with a grating ruling engine.

(the spatial period is 1000 lines/mm). The process is schematically illustrated as Fig. 1.

After that, the sample was cleaned via ultrasonic baths in acetone, absolute alcohol and deionized water for 20 min, respectively, and then dried in the drying oven at 80 °C for 2 h. Sample b was prepared in the same way as sample a except for the ultrasonic cleaning. Sample c was a Ti sheet without any pre-pattern process and sample d was a Ti sheet that was only mechanically polished. Besides, sample c and d both went through ultrasonic cleaning as sample a did. The pretreatments of these samples are showed in the following table (Table 1).

All the samples went through the anodization process in a two-electrode electrochemical cell in which the Ti sheet was used as a working electrode and a platinum sheet was used as the counter electrode. The solution of the two-electrode cell was the ethylene glycol ($C_2H_6O_2$) containing 0.5 wt.% NH_4F with 3 vol.% deionized water. These samples were anodized under a constant voltage of 60 V (provided by Itech IT6834) for 1 h. The temperature of the solution was controlled at 5 °C during the whole anodization process. The anodization current was measured and kept record by a source-meter (Keithley 2400). After anodization, all the four samples were immersed in the absolute alcohol for 24 h to clean out the organic and inorganic impurities on their surfaces, and then the samples were put into a sealed glass container and were dried in the container naturally. For the observation of the morphology and structure of the pre-patterned Ti sheets and the subsequent anodized samples, the atomic force microscope (AFM, PARK XE-100) and the field-emission scanning electron microscope (FE-SEM, FEI Sirion 200) were used to observe and record the samples' surfaces.

3. Results and discussion

The surface morphology of the mechanically micro-etched Ti sheet before anodization is showed in Fig. 2. We can find that there are lines of wedge-shaped grooves formed on the surface and the spatial period of the grooves is about 1 μm.

Fig. 3 shows the different lengths of the TiO_2 NTs grown from the four samples. The fabrication conditions of the anodization are the same for all of the samples. We can easily find that the TiO_2 NT's growth rate of the polished, mechanically etched and ultrasonically cleaned Ti sheet (sample a) is the highest. The length of the nanotubes is more than 9 μm in 1 h at the temperature of 5 °C, while the TiO_2 NTs grown from Ti sheet without any pre-pattern process (sample c) only have a little more than 2 μm in length. The length of TiO_2 NTs grown from polished, mechanically etched but without ultrasonic cleaning Ti sheet (sample b) is about the same as that grown from the Ti sheet which was only polished and ultrasonically cleaned (sample d), both are about 5.5 ± 0.3 μm in length. Fig. 4 shows the morphologies of the pre-patterned samples (sample a and sample b) after anodization. We can find that the nanostructure exists on both bottom and side walls of the grooves. At the bottom, the top of the nanotube is open. On the side walls there are similar nanotube structures. The nanotube is perpendicular to the side walls and the bottom of the nanotube is closed. We can also find that the diameter of the NTs from sample a is about 130 nm, while for sample b about 60–70 nm. The cause of the great difference in diameters between sample a and sample b had close relation to the anodization current, and we can easily point out in Fig. 6 that the anodization current of sample a is much larger than that of sample b.

As reported in former researches, it is generally accepted that the mechanism of the growth of the TiO_2 NTs lies in the competition between formation of TiO_2 and dissolution of $[TiF_6]^{2-}$ during anodization [29,30]. The reactions can be described as:

$$2H_2O \rightarrow O_2 + 4e^- + 4H^+ \quad (1)$$

$$Ti + O_2 \rightarrow TiO_2 \quad (2)$$

$$TiO_2 + 6F^- + 4H^+ \rightarrow [TiF_6]^{2-} + 2H_2O \quad (3)$$

$$Ti^{4+} + 6F^- \rightarrow [TiF_6]^{2-} \quad (4)$$

Firstly, the growth of the TiO_2 at the surface of the Ti sheet occurs due to the interaction of the Ti with O^{2-} ions. After an initial oxide layer is formed, these anions migrate through the oxide layer to the Ti/TiO_2 interface and then react with Ti as showed in reaction (1) and (2). Meanwhile, the applied electric field ejects Ti^{4+} cations from the Ti/TiO_2 interface and makes Ti^{4+} move towards the TiO_2/electrolyte interface. The chemical dissolution takes place at the interface of TiO_2/electrolyte where TiO_2 is dissolved by F^- with the help of H^+ and the field-assisted dissolution occurs at the Ti/TiO_2 interface as reaction (3) and (4) show. The NTs grow initially

Table 1
Different pretreatments of the four samples.

Sample	Polishing	Micro-etching	Ultrasonic cleaning
a	Yes	Yes	Yes
b	Yes	Yes	No
c	No	No	Yes
d	Yes	No	Yes

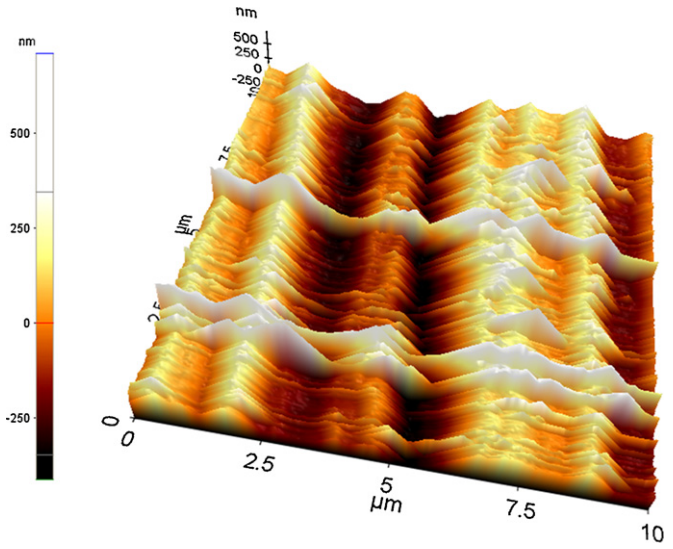

Fig. 2. AFM image of the surface of mechanically micro-etched Ti sheet. The spatial period of the grooves is about 1 μm.

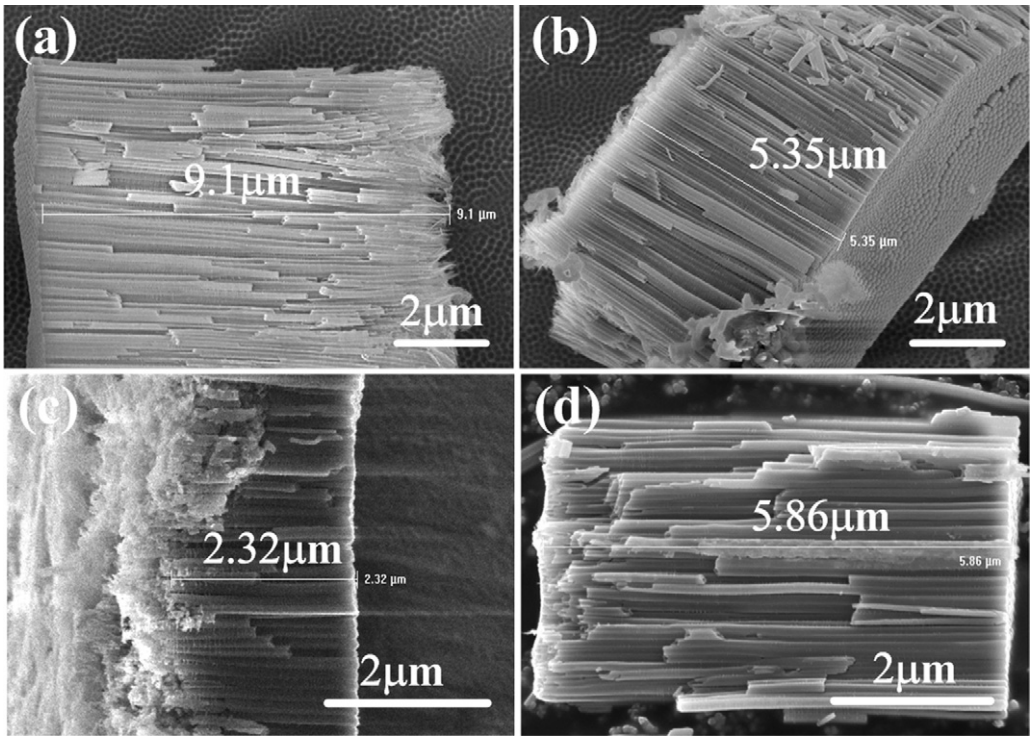

Fig. 3. SEM images of nanotube lengths of sample a, b, c and d. (a) Length of NT grew from sample a, 9.1 μm (b) Length of NT grew from sample b, 5.35 μm (c) Length of NT grew from sample c, 2.32 μm (d) Length of NT grew from sample d, 5.86 μm.

at small pits formed by the localized dissolution of the oxide, and once the oxide layer becomes thick due to the faster oxidization speed compared with the dissolution speed, the migration of the O^{2-} ions to the Ti/TiO_2 interface is weakened. Thus the oxidization process slows down because of the lack of these ions, while dissolution speed at the TiO_2/electrolyte interface does not change. In such case it makes the oxide layer become thin, and then the oxidization process speeds up again because of the thinner oxide layer

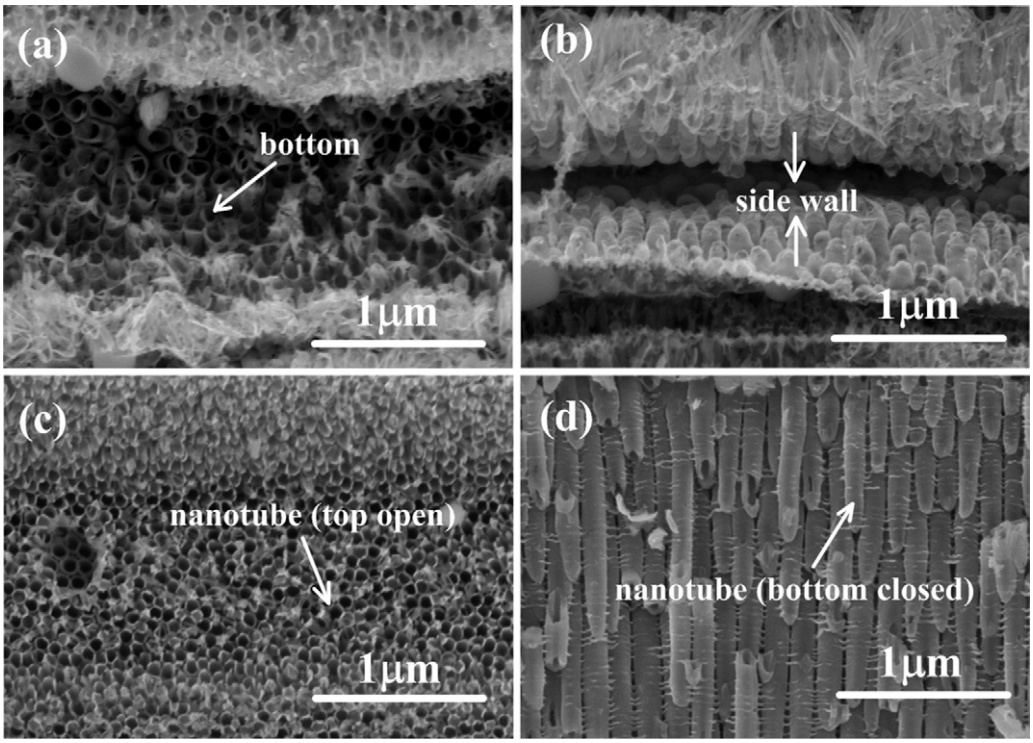

Fig. 4. SEM images of morphologies of sample a and sample b after anodization. (a) Bottom of the wall structure from sample a, diameter of the nanotube is about 130 nm. (b) Side walls of the nanostructure from sample a. (c) Morphology of NT at the bottom of the grooves from sample b. Diameter of the nanotube is about 60–70 nm.(d) Nanotubes (bottom closed) grown perpendicular to the side walls of sample b.

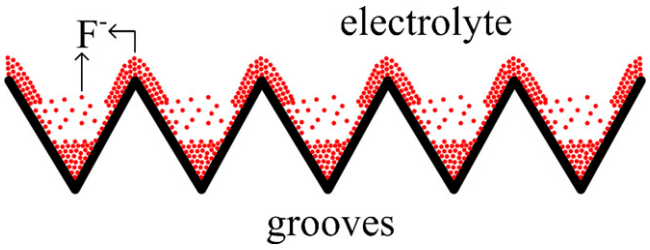

Fig. 5. Schematic illustration of the distribution of the corrosive ions (F^-) on the groove's surface when the electric field is rearranged on the surface due to the wedge-shaped morphology.

which has less obstruction effect of the O^{2-} ions' migration to the Ti/TiO_2 interface. These processes have some properties just like the negative feedback which will finally make the formation and the dissolution of the oxide layer reach an equilibrium state, thus the thickness of the oxide layer does not change anymore while the small pits become bigger and deeper converting into pores and eventually form the NTs [31].

The oxidization and the field-assisted dissolution are dominated by the electric field. In our case, for sample a, the distribution of the electric field is rearranged due to the sharp surface effect. The electric field is much stronger at the tip of the wedge-shaped grooves compared to that at the flat surface. Consequently the oxidization and field-assisted dissolution speed at that location is much greater. Meanwhile, the unevenly distributed electric field changes the distribution of the ions, such as F^-, O^{2-}, just as showed schematically in Fig. 5, making these ions concentrate in the wedge-shaped areas. This situation increases the oxidization and chemical dissolution speed, so that the overall oxidization speed and dissolution speed are raised to a higher level when they reach the new equilibrium.

For sample b, the absence of the ultrasonic cleaning process may leave the impure particles on the sample's surface that will damage the distribution of the electric field which appeared in sample a. These impurities weaken the sharp surface effect and reduce the anodization current, thus the growth speed of the NTs declines. Compared to sample c which is without any pretreatment, both sample b and sample d are polished. This pretreatment makes the roughness of the surface low, and the distribution of the electric field is relatively regular. As sample c has a rough surface, the irregular protrusions and concaves on the surface will force the electric field to distribute randomly. The anodization current is also consumed by these irregular microstructures, so the NTs' growth speed of sample c is even lower. This can be confirmed in Fig. 6 which illustrates the current densities of these samples during the anodization process.

We can find that the biggest current density exists in sample a, and sample b and d has the similar current density curve throughout the whole anodization process, while sample c has the lowest current density. After anodization process went on about hundreds of seconds, the current densities of these samples began to decline and kept at a comparatively stable state which indicated that the oxidization and the dissolution reach the equilibrium. The differences of the anodization current densities result in the different TiO_2 NTs length of the samples.

As showed in Fig. 4, sample a and b have a wall structure which is made up by NT arrays. This kind of structure is formed on the walls of the micro-etched grooves. The growth mechanism of the NT is similar to the NT formation theory discussed in the previous part. The only difference is that the nanostructure is formed by the growth of the NT on both bottom and the side walls. In this way, the wall structure increases the dimensions of the NTs' distribution and apparently it increases the surface-to-volume ratios. Thus this structure can absorb more sensitized dyes if applied in the DSSC and probably has the potential of improving the efficiency of the DSSC. Furthermore, it has the possibility in improving the efficiency of photocatalysis with its high surface-to-volume ratios characteristic.

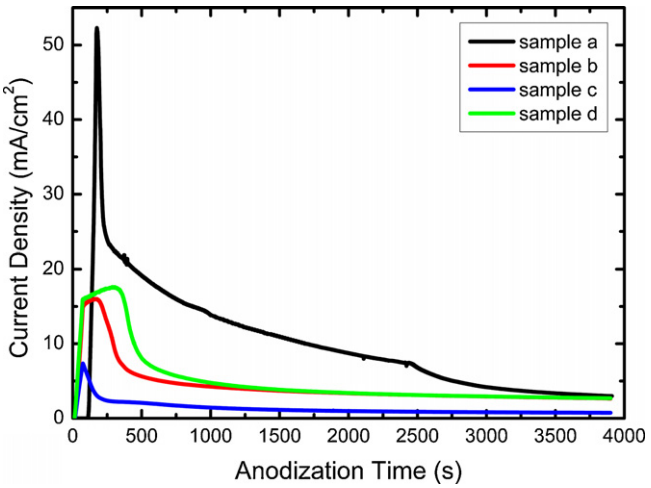

Fig. 6. Current density–anodization time curves of the samples during the anodization process.

4. Conclusions

In summary, our work presented a new method which directly etched the surface of the titanium sheet by a grating ruling engine and formed a novel nanostructure named wall structure after anodization. Besides, we find the pre-pattern (mechanical micro-etching) which formed grooves on the surface of the titanium sheet will accelerate the growth speed of the TiO_2 NTs. We also find that the ultrasonic cleaning before the anodization of the titanium sheet was important, for it will clean out the impurities on the surface of titanium sheet, preventing the impurities from interfering with the distribution of the electric field and consuming the anodization current. The newly formed wall structure maybe useful in the photovoltaic and photocatalysis field for its high surface-to-volume ratios compared with previously reported NT membrane. Meanwhile, the idea of mechanical micro-etching as pre-pattern maybe helpful in further optimization of the fast growth of TiO_2 NTs/nanostructure or the formation of the novel structures.

Acknowledgements

This research was supported by the National Natural Science Foundation of China (10874119); the National Basic Research Program "973" of China (no. 2007CB307000); the Shanghai Leading Academic Discipline Project (B201); and Instrumental Analysis Center, Shanghai Jiao Tong University.

References

[1] I.K. Konstantinou, T.A. Albanis, TiO_2-assisted photocatalytic degradation of azo dyes in aqueous solution: kinetic and mechanistic investigations: a review, Appl. Catal. B: Environ. 49 (2004) 1–14.
[2] S.P. Albu, A. Ghicov, J.M. Macak, R. Hahn, P. Schmuki, Self-organized, free-standing TiO_2 nanotube membrane for flow-through photocatalytic applications, Nano Lett. 7 (2007) 1286–1289.
[3] J.M. Macak, M. Zlamal, J. Krysa, P. Schmuki, Self-organized TiO_2 nanotube layers as highly efficient photocatalysts, Small 3 (2007) 300–304.
[4] A. Fujishima, X. Zhang, D.A. Tryk, TiO_2 photocatalysis and related surface phenomena, Surf. Sci. Rep. 63 (2008) 515–582.
[5] A. Nozik, Photoelectrolysis of water using semiconducting TiO_2 crystals, Nature 257 (1975) 383–386.

[6] O.K. Varghese, M. Paulose, K. Shankar, G.K. Mor, C.A. Grimes, Water-photolysis properties of micron-length highly-ordered titania nanotube-arrays, J. Nanosci. Nanotechnol. 5 (2005) 1158–1165.
[7] M. Radecka, TiO_2 for photoelectrolytic decomposition of water, Thin solid films 451 (2004) 98–104.
[8] C. Garzella, E. Comini, E. Tempesti, C. Frigeri, G. Sberveglieri, TiO_2 thin films by a novel sol–gel processing for gas sensor applications, Sens. Actuators B 68 (2000) 189–196.
[9] E. Traversa, M.L. Di Vona, S. Licoccia, M. Sacerdoti, M.C. Carotta, L. Crema, G. Martinelli, Sol–gel processed TiO_2-based nano-sized powders for use in thick-film gas sensors for atmospheric pollutant monitoring, J. Sol–Gel Sci. Technol. 22 (2001) 167–179.
[10] H. Tang, K. Prasad, R. Sanjinés, F. Lévy, TiO_2 anatase thin films as gas sensors, Sens. Actuators B 26 (1995) 71–75.
[11] B. O'regan, M. Gr tzel, A low-cost, high-efficiency solar cell based on dye-sensitized colloidal TiO_2 films, Nature 353 (1991) 737–740.
[12] U. Bach, D. Lupo, P. Comte, J. Moser, F. Weiss rtel, J. Salbeck, H. Spreitzer, M. Gr tzel, Solid-state dye-sensitized mesoporous TiO_2 solar cells with high photon-to-electron conversion efficiencies, Nature 395 (1998) 583–585.
[13] C.C. Chen, H.W. Chung, C.H. Chen, H.P. Lu, C.M. Lan, S.F. Chen, L. Luo, C.S. Hung, E.W.G. Diau, Fabrication and characterization of anodic titanium oxide nanotube arrays of controlled length for highly efficient dye-sensitized solar cells, J. Phys. Chem. C 112 (2008) 19151–19157.
[14] G.K. Mor, K. Shankar, M. Paulose, O.K. Varghese, C.A. Grimes, Use of highly-ordered TiO_2 nanotube arrays in dye-sensitized solar cells, Nano Lett. 6 (2006) 215–218.
[15] D.S. Koktysh, X. Liang, B.G. Yun, I. Pastoriza-antos, R.L. Matts, M. Giersig, C. Serra-odríguez, L.M. Liz-arzán, N.A. Kotov, Biomaterials by design: layer-by-layer assembled ion-elective and biocompatible films of TiO_2 nanoshells for neurochemical monitoring, Adv. Funct. Mater. 12 (2002) 255–265.
[16] L. Peng, M.L. Eltgroth, T.J. LaTempa, C.A. Grimes, T.A. Desai, The effect of TiO_2 nanotubes on endothelial function and smooth muscle proliferation, Biomaterials 30 (2009) 1268–1272.
[17] Z. Miao, D. Xu, J. Ouyang, G. Guo, X. Zhao, Y. Tang, Electrochemically induced sol–gel preparation of single-crystalline TiO_2 nanowires, Nano Lett. 2 (2002) 717–720.
[18] D.M. Antonelli, J.Y. Ying, Synthesis of hexagonally packed mesoporous TiO_2 by a modified sol–gel method, Angew. Chem. Int. Ed. 34 (1995) 2014–2017.
[19] M. Paulose, K. Shankar, S. Yoriya, H.E. Prakasam, O.K. Varghese, G.K. Mor, T.A. Latempa, A. Fitzgerald, C.A. Grimes, Anodic growth of highly ordered TiO_2 nanotube arrays to 134 μm in length, J. Phys. Chem. B 110 (2006) 16179–16184.
[20] D.S. Kim, S.Y. Kwak, The hydrothermal synthesis of mesoporous TiO_2 with high crystallinity, thermal stability, large surface area, and enhanced photocatalytic activity, Appl. Catal., A 323 (2007) 110–118.
[21] S. Liu, K. Huang, Straightforward fabrication of highly ordered TiO_2 nanowire arrays in AAM on aluminum substrate, Sol. Energy Mater. Sol. Cells 85 (2005) 125–131.
[22] H. Masuda, K. Kanezawa, M. Nakao, A. Yokoo, T. Tamamura, T. Sugiura, H. Minoura, K. Nishio, Ordered arrays of nanopillars formed by photoelectrochemical etching on directly imprinted TiO_2 single crystals, Adv. Mater. 15 (2003) 159–161.
[23] S.D. Burnside, V. Shklover, C. Barbé, P. Comte, F. Arendse, K. Brooks, M. Gr tzel, Self-organization of TiO_2 nanoparticles in thin films, Chem. Mater. 10 (1998) 2419–2425.
[24] S.Z. Chu, S. Inoue, K. Wada, S. Hishita, K. Kurashima, Self-Organized Nanoporous Anodic Titania Films and Ordered Titania Nanodots/Nanorods on Glass, Adv. Funct. Mater. 15 (2005) 1343–1349.
[25] G.K. Mor, O.K. Varghese, M. Paulose, C.A. Grimes, Transparent highly ordered TiO_2 nanotube arrays via anodization of titanium thin films, Adv. Funct. Mater. 15 (2005) 1291–1296.
[26] H. Masuda, H. Yamada, M. Satoh, H. Asoh, M. Nakao, T. Tamamura, Highly ordered nanochannel-array architecture in anodic alumina, Appl. Phys. Lett. 71 (1997) 2770.
[27] J. Choi, R.B. Wehrspohn, J. Lee, U. Gosele, Anodization of nanoimprinted titanium: a comparison with formation of porous alumina, Electrochim. Acta 49 (2004) 2645–2652.
[28] J. Qiu, Z. Jin, Z. Liu, X. Liu, G. Liu, W. Wu, X. Zhang, X. Gao, Fabrication of TiO_2 nanotube film by well-aligned ZnO nanorod array film and sol–gel process, Thin solid films 515 (2007) 2897–2902.
[29] J. Macak, H. Tsuchiya, A. Ghicov, K. Yasuda, R. Hahn, S. Bauer, P. Schmuki, TiO_2 nanotubes: Self-organized electrochemical formation properties and applications, Curr. Opin. Solid State M. 11 (2007) 3–18.
[30] J. Macak, H. Hildebrand, U. Marten-Jahns, P. Schmuki, Mechanistic aspects and growth of large diameter self-organized TiO_2 nanotubes, J. Electroanal. Chem. 621 (2008) 254–266.
[31] G.K. Mor, O.K. Varghese, M. Paulose, K. Shankar, C.A. Grimes, A review on highly ordered, vertically oriented TiO_2 nanotube arrays: fabrication material properties, and solar energy applications, Sol. Energy Mater. Sol. Cells 90 (2006) 2011–2075.